Submitted to Chapman Conference on Magnetic Helicity: September 30, 1998.

Solar-Cycle, Radial and Latitudinal Variations of Magnetic Helicity: IMF Observations

Charles W. Smith

Bartol Research Institute, University of Delaware, Newark

Abstract. Solar wind dynamics span an extensive range of spatial scales from greater than an AU to less than the gyroradius of a thermal proton. Throughout this range there exist dynamics that lead to the creation, annihiliation and transport of magnetic helicity. This paper examines some of these processes with measurements of the interplanetary magnetic helicity. We find both kinetic plasma processes as well as MHD and solar source dynamics that lead to magnetic helicity in the solar wind. We attempt to characterize the interplanetary magnetic helicity with a combination of review and new material.

1. Introduction

In situ measurements of the interplanetary magnetic field (IMF) now span more than 35 years of spacecraft observations since the launch of IMP-1 in 1963. Coverage of the near-Earth IMF has been sufficient to permit long-term studies of the solar-cycle variability of the field [*King*, 1976; *Smith and Bieber*, 1991, 1993; *King and Papitashvili*, 1994]. In the 1970s the interplanetary missions of Pioneer 10 & 11 [*Hall*, 1974] and Voyagers 1 & 2 [*Behannon et al.*, 1977] created the opportunity to study the more distant outer heliosphere. Most recently, Ulysses [*Balogh et al.*, 1992] has provided the first in situ observations of the IMF and helicity over the solar poles [*Goldstein et al.*, 1995]. This paper attempts to summarize the basic observations of magnetic helicity of the IMF. A complete review is impossible within the confines of this article, so we will instead attempt to capture the fundamental attributes of the IMF magnetic helicity.

To begin, we must first acknowledge that the *Parker* [1963] winding of the IMF spiral contains helicity [*Bieber et al.*, 1987]. Helicity at this scale results from nothing more than the freezing of the IMF into the radially expanding flow coupled with the rotation of the solar corona. This helicity exhibits a persistent and steady south–north asymmetry > 0 wherein the two heliospheric hemispheres display helicity of different signs and equal magnitude.

The range of spatial and temporal scales for IMF variability in the solar wind are as extensive as the measurements themselves. For spatial scales greater than the measurement's heliocentric distance (spacecraft frame frequencies less than 4×10^{-6} Hz for measurements recorded at 1 AU) the spectrum is entirely and undisputably a manifestation of the variability of the solar source. At higher frequencies, extending to time scales of a few hours (10^{-4} Hz) the interplanetary power spectrum at 1 AU possesses an f^{-1} form. This range, which we will call the source range, is thought to result from the influence of many, uncorrelated solar sources [*Matthaeus and Goldstein*, 1986]. Figure 1 shows the high-frequency end of this range. At still higher frequencies, from 3×10^{-5} Hz (time scales on the order of 1 hour) to ~ 0.5 Hz (not shown) is the inertial range which possesses an $f^{-5/3}$ power law form. In most cases the inertial range extends to frequencies more comparable to 1×10^{-5} Hz and may as well in this instance, but with poor resolution. Drawing on a simple analogy with hydrodynamics, the inertial range is thought to be an energy-conserving conduit for energy cascading from larger spatial scales down to the smallest scales for dissipation. At still higher frequencies the spectrum steepens and dissipation of magnetic energy occurs.

Following a description of how the magnetic helicity is measured in the solar wind, we present the results of recent studies of the IMF dissipation range. Then, building through the inertial range to larger scales, we will close this paper by showing the persistent south–north asymmetry of magnetic helicity at scales that are smaller than the Parker winding scale

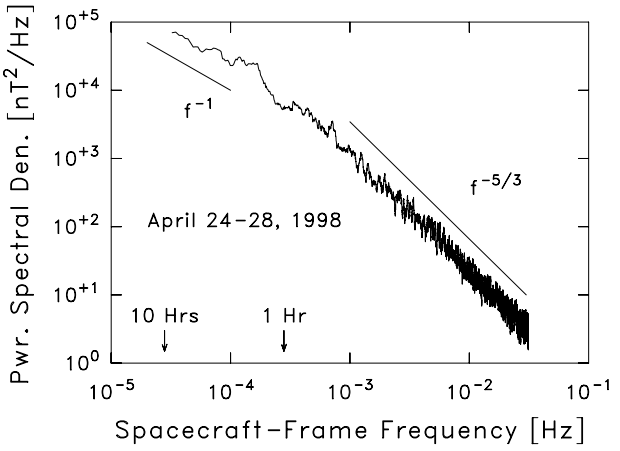

Figure 1. A fairly typical magnetic power spectrum for quiet solar wind conditions as observed by the ACE spacecraft. Only the N component of the field was used. The $f^{-5/3}$ power-law of the inertial range is clearly evident as is the high-frequency end of the f^{-1} range. The spacecraft frequencies for signals spanning 1 hour and 10 hours in spacecraft data are shown at the bottom.

but larger than the inertial range fluctuations.

2. Method

The method for measuring the magnetic helicity in homogeneous, turbulent magnetofluids [*Matthaeus and Smith*, 1981; *Matthaeus et al.*, 1982; and *Oughton et al.*, 1997] is derived from the two-point autocorrelation function

$$R_{ij} \equiv \langle b_i(\mathbf{x}) b_j(\mathbf{x}+\mathbf{r}) \rangle \qquad (1)$$

where $b_i(\mathbf{x}) \equiv B_i(\mathbf{x}) - \langle B_i(\mathbf{x}) \rangle$ is the i^{th} component of the fluctuating magnetic field resulting from the subtraction of the mean field from the measurement. The ensemble average $\langle \ldots \rangle$ is typically computed from a spatial or temporal average. It is then possible to define a function

$$2\Phi(\mathbf{r}) = \int_{\infty}^{\mathbf{r}} dr \left[R_{ij}(\mathbf{r}) - R_{ji}(\mathbf{r}) \right] \qquad (2)$$

where the direction given by $\mathbf{r}$ is arbitrary, but the components i and j represent directions normal to $\mathbf{r}$ such that $\hat{\mathbf{i}} \times \hat{\mathbf{j}} = \hat{\mathbf{r}}$. It is customary to define IMF measurements in heliocentric (R, T, N) components where $\hat{\mathbf{R}}$ is directed radially outward from the sun, $\hat{\mathbf{T}}$ is coplanar to the sun's rotational equator and directed in the sense of rotation, and $\hat{\mathbf{N}} = \hat{\mathbf{R}} \times \hat{\mathbf{T}}$. Since the solar wind flow is both supersonic and super-Alfvénic in the $\hat{\mathbf{R}}$ direction, it is customary to assume that the magnetic fluctuations are frozen into the flow and rewrite equation 2 in terms of temporal lags along the solar wind flow:

$$2\Phi(t) = \int_{\infty}^{t} d\tau \, (V_{SW}) \left[R_{TN}(\tau) - R_{NT}(\tau) \right]. \qquad (3)$$

From either equations 2 or 3 we can obtain the net magnetic helicity in the Coulomb gauge:

$$H_M = 2\Phi(0). \qquad (4)$$

We can obtain the reduced wavenumber spectrum of magnetic helicity from the spectral decomposition of the autocorrelation function according to

$$S_{ij}(k_r) \equiv (2\pi)^{-1} \int d\tau e^{-ik_r r} R_{ij}(r) \qquad (5)$$

and from this the helicity spectrum is obtained to be

$$H_M(k_r) = (-i) \left[S_{TN}(k_r) - S_{NT}(k_r) \right] (k_r)^{-1} \qquad (6)$$

In the above, k_r is the reduced wavenumber and decomposition is performed only along the flow direction. The magnetic helicity spectrum can be constrained according to the minimum energy required to support the helicity so that we can define

$$\sigma_M(k_r) = k_r \frac{H_M(k_r)}{E_B(k_r)} \qquad (7)$$

where $E_B(k_r) \equiv \Sigma_i [S_{ii}(k_r)]$ and $-1 \leq \sigma_M(k_r) \leq +1$.

The definition of the magnetic helicity is fundamentally a spatial concept, so the above definitions have been written in terms of a reduced wavenumber. To make contact with solar wind observations, we will convert the reduced wavenumber to frequency according to

$$f = k_r V_{SW} / 2\pi \qquad (8)$$

and write

$$\sigma_M(f) = \frac{2\pi f}{V_{SW}} \frac{H_M(f)}{E_B(f)} \qquad (9)$$

for the normalized magnetic helicity spectrum.

3. Dissipation Range

Recent analyses of the magnetic helicity in the dissipation range [*Goldstein et al.*, 1994; *Leamon et al.*, 1998a] reveal significant magnetic helicity signatures. A typical observation of a magnetic helicity spectrum associated with IMF dissipation is shown in Figure 2

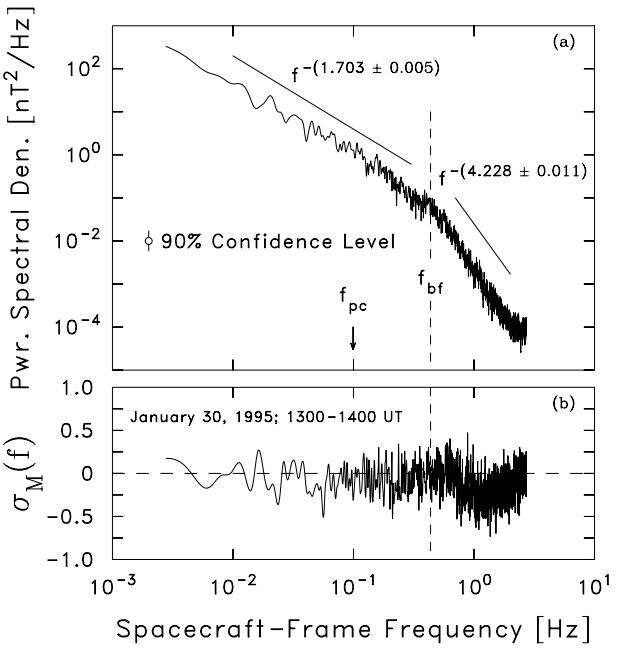

Figure 2. Power spectrum (top) and magnetic helicity spectrum (bottom) for a typical interval of WIND observations of the undisturbed solar wind at 1 AU near zero heliographic latitude. Figure reprinted from *Leamon et al.* [1998a].

where a 30% bias of $\sigma_M(f)$ is observed within the dissipation range. Nonzero magnetic helicity is one signature of cyclotron resonance. *Leamon et al.* [1998b, c] show that other processes, most notably ion and electron Landau damping, are also present. Electron Landau damping accounts for $\sim 1/2$ of the total dissipation, thereby providing heating of the thermal electrons as well as the thermal ions heated through the cyclotron and ion-Landau resonances. These processes and the magnetic helicity feature shown in Figure 2 are ubiquitous within the solar wind, although further study is needed to resolve the relative importance of these processes in the outer heliosphere.

Under similar circumstances where wave-particle interactions are key, magnetic helicity signatures can easily be generated. Examples include upstream dynamics at shocks [*Smith et al.*, 1983; 1985] where energetic beams excite low-frequency fluctuations within the inertial range [*Lee*, 1984] and the waves due to pickup ions of cometary [*Tsurutani*, 1991; *Yoon and Wu*, 1991] or interstellar [*Lee and Ip*, 1987] origin. Unlike these cases where wave energy is excited, the helicity signatures present in the dissipation range result from the kinetic damping of one polarization over another in a wave field where a single propagation direction is preferred [*Leamon et al.*, 1998b]. Magnetic helicity is easily generated at energetically significant levels when non-MHD processes are involved.

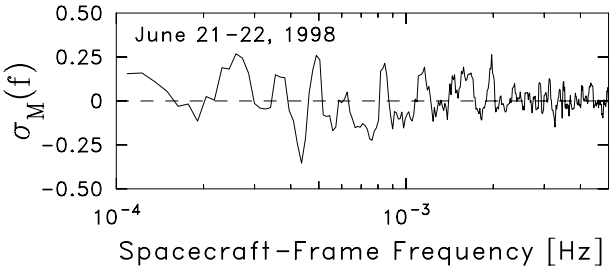

Figure 3. Normalized magnetic helicity spectrum $\sigma_M(f)$ for a frequency interval within the inertial range as recorded by ACE using 10 degrees of freedom. More aggressive smoothing to achieve higher degrees of freedom will eventually drive the spectrum to zero.

4. Inertial Range

The most curious aspect of the inertial range is that any given frequency is likely to have an energetically significant amount of magnetic helicity [*Matthaeus and Goldstein*, 1982], but no net helicity exists within this range when integrated over the full frequency range or a significant fraction of the full range. An example of an inertial range spectrum is shown in Figure 3.

Matthaeus and Goldstein [1982] demonstrate that this behavior is observed out to 5 AU in the Voyager dataset and subsequent analyses [e.g., *Goldstein et al.*, 1994] continue to confirm this result wherever the inertial range helicity has been measured. The only exception to this, as noted above, is when kinetic effects excite waves of a single helicity over a limited range of the spectrum for limited times.

5. Sources Range

In this section we show figures based both on results from equation 4 and the integrand in equation 3. It should be noted that symmetry considerations, homogeneity and integrability dictate that

$$[R_{TN}(\tau) - R_{NT}(\tau)] \stackrel{\tau \to 0}{\longrightarrow} 0 \text{ (symmetry)} \quad (10)$$

$$\stackrel{\tau \to \infty}{\longrightarrow} 0 \text{ (integrability)} \quad (11)$$

There are potentially two additional complications to the study proposed here. First, there exist large-scale reversals of the IMF in the near-ecliptic called

magnetic sectors which are associated with crossings of the heliospheric current sheet (HCS) [*Ness and Wilcox*, 1965]. Analyzing the data without regard for sector structure represents both a potential large-amplitude "noise" signal which may contaminate the analysis of low-frequency fluctuations and the admixture of potentially unrelated observations. To this end, observations of magnetic field reversals represent the passage of the spacecraft between field lines connected to different solar hemispheres. Both removal of this signal and separation of the two measurement types are desirable. We therefore separate the IMF measurements into "toward" and "away" sector types using the expected *Parker* [1963] spiral direction [*Smith and Bieber*, 1991, 1993; *Smith and Phillips*, 1997] and separately analyze the two populations.

Second, IMF intensity variations associated either with solar-cycle, radial or latitudinal variations of the interplanetary medium can complicate comparisons of magnetic helicity results for different times or different locations. While we have developed a means of addressing this problem, it is too convoluted for presentation here. For this reason, we will simply cite the results for analyses of outer heliosphere and high-latitude datasets.

An intermediate timescale, which we take to be one solar rotation, is used to compute statistically independent estimates of the helicity. These intermediate estimates are then averaged over longer time intervals, which we generally take to be 1 year or longer, in order to obtain statistical uncertainties and refined estimates of the mean helicity asymmetry.

We impose one further constraint on the data: We demand that each estimate of the correlation function (the integrand in equation 3) obtained for a given intermediate interval be the result of at least 20 individual products of the measurements at every lag. This insures adequate coverage and reduces the likelihood that a poorly-sampled correlation function will adversely affect the resulting average. Any estimate of the correlation function derived for an individual intermediate time interval that fails to meet this criterion is discarded.

5.1. Net Helicity

We can employ the methods discussed in section 2 to compute the temporal behavior of the low-frequency magnetic helicity at 1 AU and near-ecliptic latitudes using the National Space Science Data Center (NSSDC) Omnitape dataset. The temporal resolution of Omnitape data is 1 hour. The practical concern of making a measurement requires that we limit the maximum lag in equations 2 and 3 to finite values. We will use a 36-hour maximum lag in the estimation of Φ and justify this assumption in section 5.2.

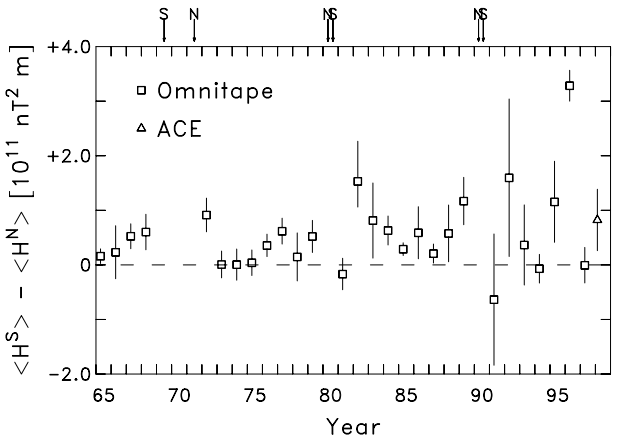

Figure 4. Net helicity asymmetry (south–north) as recorded on the Omnitape (squares) and ACE (triangle) datasets. Error estimates are determined from intermediate timescale (individual solar rotation) estimates of the asymmetry. The times of the solar magnetic reversals of the north (N) and south (S) solar poles are marked at the top of the figure.

We subtract the computed helicities for northern heliospheric hemisphere measurements from those of the south making use of the association between sector polarity and the solar magnetic dipole state. Because the solar magnetic dipole is ill-defined from 1969–71 and in 1980 and 1990, we must discard these years from the analysis. The results are shown in Figure 4. We add to the Omnitape results measurements recorded by the Advanced Composition Explorer (ACE) spacecraft, which was launched in August 1997. ACE measurements, represented as a triangle in Figure 4, from shortly after launch until the end of June 1998 were used.

The striking conclusion of Figure 4 is that there exists a persistent south–north > 0 asymmetry in the net magnetic helicity of the IMF that spans 34 years of observations (neglecting the 5 years when the solar polarity is ill-determined) with only 4 exceptions (and all 4 exceptions are equivalent to zero to within 1 estimated error of the mean). The average south–north asymmetry for the magnetic helicity as computed by this method using the Omnitape dataset from 1965 through 1997 is $(4.51 \pm 1.09) \times 10^{10}$ nT^2 m. *Bieber* [this volume] discusses the implications this result holds for the propagation of cosmic rays in the interplanetary medium.

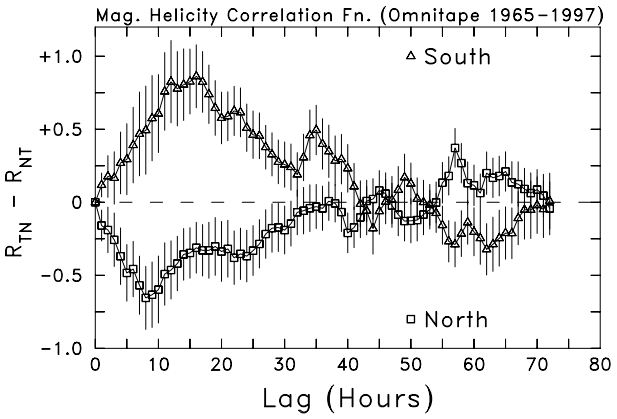

Figure 5. Integrand of $\Phi(t)$ as computed from the Omnitape dataset for the years 1965–1997, excluding the years of solar magnetic dipole reversal. The correlation function for the northern (squares) and southern (triangles) hemispheric measurements are determined separately. The statistical uncertainty is obtained from the intermediate-timescale analysis.

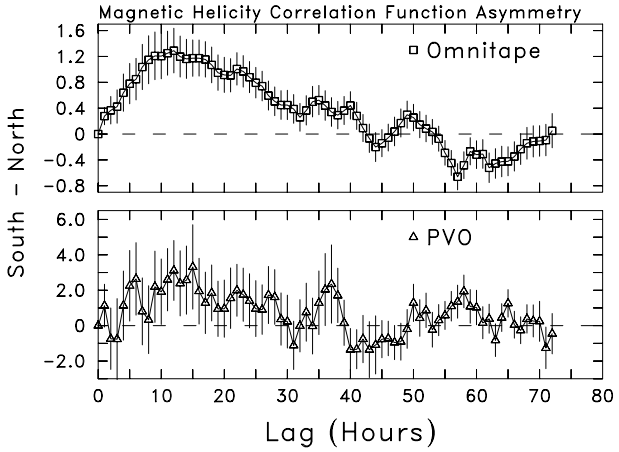

Figure 6. (top) Difference between southern and northern hemispheric corellation functions as shown in Fig. 5. The same quantity is computed from PVO observations (bottom) for the years 1978–89. Note change in scale.

Although not shown here, the Pioneer-Venus Orbiter observations from 0.7 AU and 1978–89 as well as Pioneer 10 observations from 1973–75 and 1–6 AU, Pioneer 11 observations from 1974–79 and 1–8 AU, Voyager 1 & 2 observations from 1977–84 and 1–18 AU and Ulysses observations from 1991–92 and 2–5 AU all support this basic conclusion. The IMF fluctuation intensity decreases with increasing heliocentric distance, but in all of the above cases the relative amount of helicity scales roughly with the magnetic energy to within a factor of $\sim$2. There is only minimal evidence that some degree of helicity injection or accumulation is active in the interplanetary medium at these scales and adding to the helicity seen at 1 AU. This evidence comes from the years 1973-75 when no magnetic helicity asymmetry is observed at 1 AU, but a finite amount of helicity with low statistical significance can be seen in the Pioneer 10 dataset. In this case, the asymmetry observed agrees with the overall results of Figure 4.

5.2. Correlation Functions

In this section we accomplish 3 things: First, we justify the assumption that a 36-hour maximum lag is sufficient to assess the net magnetic helicity at 1 AU. Second, we show that the average helicity computed across the HCS is zero. Third, we uncover a minor helicity signal associated with longer lags that is interesting, but excluded from the above results.

The first indication that the maximum lag is sufficient comes from recomputing the average asymmetry for the Omnitape dataset using a 72 hour maximum lag. The result is $(3.08 \pm 1.13) \times 10^{10}$ nT^2 m. This slightly reduced result suggests a possible feature at lags longer than 36 hours, but does not undo the earlier conclusions.

We can extract the integrand from equation 3 and neglect the factor of V_{SW}. Figure 5 shows computed values of this term separately for northern (squares) and southern (triangles) hemispheric measurements. The significant feature for 1–30 hour lags is evident in approximately equal and oppositely signed values of the correlation functions. This is the aspect of the correlation function that leads to the computed and persistent south–north asymmetry plotted in Figure 4. Figure 5 also demonstrates that the average H_M computed across the current sheet is approximately zero due to the approximate cancellation of these two features when summed.

The next interesting aspect of Figure 5 is the apparent reversal of the correlation functions at about 50-hour lags that results in an oppositely-signed helicity asymmetry at 50–70 hour lags. This is the feature that caused the above decrease in the computed helicity asymmetry for maximum lags of 72 hours.

The convection time for the solar wind to reach from the sun to the Earth is about 97 hours at 427 km/s (the mean wind speed for the Omnitape dataset). Therefore, any feature at lags greater than this must be a solar source effect and we choose to neglect these larger lags in this discussion. *Matthaeus*

[this volume] argues that any structure greater than ~ 0.1 AU (10-hour lags) cannot arise from collective processes such as inverse cascade and must be a solar source effect. Therefore, it seems likely that the helicity asymmetry shown here and in Figure 4 is the result of solar sources and is not the result of processes such as inverse cascade working in the interplanetary medium.

We complete the connection with Figure 4 by subtracting the northern correlation functions from the southern forms. This is shown in Figure 6. Here, again, the helicity feature associated with lags < 30 hours is clearly evident at high statistical significance. The same quantity is computed from PVO observations for the years 1978–89 to demonstrate the reproducibility of this result. The higher levels of the correlation function for the PVO results are associated with greater IMF intensity at 0.7 AU while the greater uncertainties are the result of using fewer years in the average.

5.3. CMEs

Coronal mass ejections (CMEs), which are generally diagnosed in interplanetary datasets through the observation of counterstreaming suprathermal electrons [*Gosling et al.*, 1987], are often observed in association with magnetic clouds [*Klein and Burlaga*, 1982; *Burlaga et al.*, 1990; *Gosling*, 1990]. Clouds are twisted flux ropes [*Burlaga et al.*, 1981; *Farrugia et al.*, 1995] that have relaxed to nearly force-free states [*Goldstein*, 1983; *Marubashi*, 1986; *Farrugia et al.*, 1992]. As such, they carry magnetic helicity at large spatial scales.

Bieber and Rust [1995] suggest that the helicity asymmetry at the large scales is the result of solar helicity injection through CMEs. *Rust* [1994] observes that magnetic clouds possess the same sign of magnetic helicity as do the filaments with which they are associated, so it is possible that there exist other sources of low-frequency magnetic helicity in the low-speed solar wind that originates from the streamer belt region [*Rust and Kumar*, 1996].

A preliminary examination of ISEE-3 observations (not shown here) using a catalog of CMEs for this spacecraft [J. T. Gosling, private communication, 1996] has revealed that half of the magnetic helicity shown in Figures 4 – 6 can be eliminated by the removal of CMEs from the dataset. Since not all magnetic clouds are coincident with CME observations, and since it is likely that the observed magnetic helicity resides within the force-free magnetic cloud configurations, it is possible that a further listing of magnetic cloud events will refine the source identification. Lastly, examination of Ulysses observations from over the solar poles (not shown) reveals very little magnetic helicity at the multi-hour scales, which is consistent with the further reduction of the signal by removal of low-speed wind originating in the streamer belt region.

6. Summary

The magnetic helicity within the solar wind is observed over a very broad range of spatial scales from *Parker* [1963] spiral that defines the magnetic structure of interplanetary space, through fluctuations on the scale of 1 AU, to the smallest scales of the dissipation range. There is minimal evidence for solar sources ejecting magnetic helicity into the wind. With nonzero helicity sources at the largest and smallest scales, the intermediate scale of the inertial range appears to act as an energy- and helicity-conserving conduit for spectral transfer without buildup of helicity within its range. While processes such as inverse cascade and relaxation to force-free states are seen to be active in the evolution of CMEs, any global transfer of helicity within the undisturbed solar wind remains only speculative.

Acknowledgments. The Bartol Research Insitute is the lead institution for the magnetic field experiments on the Voyagers and ACE. This work was supported by NASA through Ulysses Guest Investigator grant NAG5-6570, CalTech subcontract PC251439 (ACE), and Jet Propulsion Laboratory contract 959167 (Voyager) to the Bartol Research Institute.

References

Balogh, A., T. J. Beek, R. J. Forsyth, P. C. Hedgecock, R. J. Marquedant, E. J. Smith, D. J. Southwood, and B. T. Tsurutani, The magnetic field investigation on the Ulysses spacecraft: Instrumentation and preliminary scientific results, *Astron. Astrophys. Supp.*, *92*, 221–236, 1992.

Behannon, K. W., M. H. Acuña, L. F. Burlaga, R. P. Lepping, N. F. Ness, and F. M. Neubauer, Magnetic field experiment for Voyagers 1 and 2, *Space Science Reviews*, *21*, 235–257, 1977.

Bieber, J. W., Role of magnetic helicity in cosmic ray scattering, *this volume*, 1998.

Bieber, J. W., and D. M. Rust, The escape of magnetic flux from the Sun, *Astrophys. J.*, *453*, 911–918, 1995.

Bieber, J. W., P. Evenson, and W. H. Matthaeus, Magnetic helicity of the Parker spiral, *Astrophys. J.*, *315*, 700–705, 1987.

Burlaga, L. F., E. Sittler, F. Mariani and R. Schwenn, Magnetic loop behind an interplanetary shock: Voy-

ager, Helios and IMP-8 observations, *J. Geophys. Res.*, *86*, 6673–6684, 1981.

Burlaga, L. F., R. P. Lepping and J. A. Jones, Global configuration of a magnetic cloud, in *Physics of Magnetic Flux Ropes*, Geophys. Monogr. Ser., vol. 58, edited by C. T. Russell, E. R. Priest, and L. C. Lee, pp. 373–377, AGU, Washington, D.C., 1990.

Farrugia, C. J., L. F. Burlaga, P. Freeman, R. P. Lepping and V. Osherovich, A comparative study of expanding force-free constant alpha magnetic configurations with application to magnetic clouds, in Solar Wind Seven, ed. by E. Marsch and R. Schwenn, pp. 611–614, Pergamon Press, New York, 1992.

Farrugia, C. J., V. A. Osherovich and L. F. Burlaga, The magnetic flux rope versus the spheromak as models for interplanetary magnetic clouds, *J. Geophys. Res.*, *100*, 12,293–12,306, 1995.

Goldstein, H., On the field configuration in magnetic clouds, *Solar Wind 5*, NASA Conference Publ. 2280, edited by M. Neugebauer, pp. 731–733, 1983.

Goldstein, B. E., E. J. Smith, A. Balogh, T. S. Horbury, M. L. Goldstein, and D. A. Roberts, Properties of magnetohydrodynamic turbulence in the solar wind as observed by Ulysses at high heliographic latitude, *Geophys. Res. Lett.*, *22*, 3393–3396, 1995.

Goldstein, M. L., D. A. Roberts, and C. A. Fitch, Properties of the fluctuating magnetic helicity in the inertial and dissipation ranges of solar wind turbulence, *J. Geophys. Res.*, *99*, 11,519–11,538, 1994.

Gosling, J. T., Coronal mass ejections and magnetic flux ropes in interplanetary space, in *Physics of Magnetic Flux Ropes*, Geophys. Monogr. Ser., vol. 58, edited by C. T. Russell, E. R. Priest, and L. C. Lee, pp. 343-364, AGU, Washington, D.C., 1990.

Gosling, J. T., D. N. Baker, S. J. Bame, W. C. Feldman, and R. D. Zwickl, Bidirectional solar wind electron heat flux events, *J. Geophys. Res.*, *92*, 8519-8535, 1987.

Hall, C. F., Pioneer 10, *Science*, *183*, 301–302, 1974.

King, J. H., A survey of long-term interplanetary magnetic field variations, *J. Geophys. Res.*, *81*, 653–660, 1976.

King, J. H., and N. E. Papitashvili, Interplanetary Medium Data Book — Supplement 5, 1988–1993, (Rep. NSSDC/WDC–A–R&S 94–08, NASA, Greenbelt, Md) 1994.

Klein, L. W., and L. F. Burlaga, Interplanetary magnetic clouds at 1 AU, *J. Geophys. Res.*, *87*, 613–624, 1982.

Leamon, R. J., C. W. Smith, N. F. Ness, W. H. Matthaeus and H. K. Wong, Observational constraints on the dynamics of the interplanetary magnetic field dissipation range, *J. Geophys. Res.*, *103*, 4775–4787, 1998a.

Leamon, R. J., W. H. Matthaeus, C. W. Smith and H. K. Wong, Contribution of cyclotron-resonant damping to kinetic dissipation of interplanetary turbulence, *Astophys. J. Lett.*, submitted, 1998b.

Leamon, R. J., C. W. Smith, N. F. Ness and H. K. Wong, Dissipation Range dynamics: Kinetic Alfvén waves, *J. Geophys. Res.*, submitted, 1998c.

Lee, M. A., Particle acceleration and MHD wave excitation upstream of interplanetary shocks, *Adv. Space Res.*, *4*, 295–304, 1984.

Lee, M. A., and W.-H. Ip, Hydromagnetic wave excitation by ionized interstellar hydrogen and helium in the solar wind, *J. Geophys. Res.*, *92*, 11,041–11,052, 1987.

Marubashi, K., Structure of the interplanetary magnetic clouds and their solar origins, *Adv. Space Sci.*, *6*, 335, 1986.

Matthaeus, W. H., Helicity in the interplanetary B field, *this volume*, 1998.

Matthaeus, W. H. and M. L. Goldstein, Measurement of the rugged invariants of magnetohydrodynamic turbulence in the solar wind, *J. Geophys. Res.*, *87*, 6011–6028, 1982.

Matthaeus, W. H., and M. L. Goldstein, Low-frequency $1/f$ noise in the interplanetary magnetic field, *Phys. Rev. Lett.*, *57*, 495–498, 1986.

Matthaeus, W. H., and C. W. Smith, Structure of correlation tensors in homogeneous anisotropic turbulence, *Phys. Rev.*, *A24*, 2135–2144, 1981.

Ness, N. F., and J. M. Wilcox, Sector structure of the quiet interplanetary magnetic field, *Science*, *148*, 1592–1594, 1965.

Oughton, S., K.-H. Rädler, and W. H. Matthaeus, General second-rank correlation tensors for homogeneous magnetohydrodynamic turbulence, *Phys. Rev. E*, *56*, 2875–2888, 1997.

Parker, E. N., *Interplanetary Dynamical Processes*, Wiley-Interscience, New York, 1963.

Russell, C. T., and M. M. Hoppe, Upstream waves and particles, *Space Science Reviews*, *34*, 155–172, 1983.

Rust, D. M., Spawning and shedding helical magnetic fields in the solar atmosphere, *Geophys. Res. Lett.*, *21*, 241, 1994.

Rust, D. M. and A. Kumar, Evidence for helically kinked magnetic flux ropes in solar eruptions, *Astrophys. J. Lett.*, *464*, L199, 1996.

Smith, C. W., and J. W. Bieber, Solar cycle variation of the interplanetary magnetic field spiral, *Astrophys. J.*, *370*, 435–441, 1991.

Smith, C. W., and J. W. Bieber, Multiple spacecraft survey of the north-south asymmetry of the interplanetary magnetic field, *J. Geophys. Res.*, *98*, 9401–9415, 1993.

Smith, C. W., and J. L. Phillips, The role of coronal mass ejections and interplanetary shocks in interplanetary magnetic field statistics and solar magnetic flux ejection, *J. Geophys. Res.*, *102*, 249–261, 1997.

Smith, C. W., M. L. Goldstein, and W. H. Matthaeus, Turbulence analysis of the Jovian upstream 'wave' phenomenon, *J. Geophys. Res.*, *88*, 5581-5593, 1983. (Correction, *J. Geophys. Res.*, *89*, 9159–9160, 1984.)

Smith, C. W., M. L. Goldstein, S. P. Gary, and C. T. Russell, Beam driven ion cyclotron harmonic resonances in the terrestrial foreshock, *J. Geophys. Res.*, *90*, 1429–

1434, 1985.

Tsurutani, B. T., Comets: A laboratory for plasma waves and instabilities, in *Cometary Plasma Processes*, Geophys. Monogr. Ser., vol. 61, edited by A. D. Johnstone, pp. 189–209, AGU, Washington, D.C., 1991.

Yoon, P. H., and C. S. Wu, Ion pickup by the solar wind via wave-particle interactions, in *Cometary Plasma Processes*, Geophys. Monogr. Ser., vol. 61, edited by A. D. Johnstone, pp. 241–258, AGU, Washington, D.C., 1991.

C.W. Smith, Bartol Research Institute, University of Delaware, Newark, DE 19716.
(e-mail: chuck@bartol.udel.edu)

This preprint was prepared with AGU's LaTeX macros v4. File chapman98 formatted December 28, 1998.

With the extension package 'AGU^{++}', version 1.2 from 1995/01/12